

Compact quantum gates on electron-spin qubits assisted by diamond nitrogen-vacancy centers inside cavities*

Hai-Rui Wei and Fu-Guo Deng[†]

*Department of Physics, Applied Optics Beijing Area Major Laboratory,
Beijing Normal University, Beijing 100875, China*

(Dated: January 2, 2022)

Constructing compact quantum circuits for universal quantum gates on solid-state systems is crucial for quantum computing. We present some compact quantum circuits for a deterministic solid-state quantum computing, including the CNOT, Toffoli, and Fredkin gates on the diamond nitrogen-vacancy centers confined inside cavities, achieved by some input-output processes of a single photon. Our quantum circuits for these universal quantum gates are simple and economic. Moreover, additional electron qubits are not employed, but only a single-photon medium. These gates have a long coherent time. We discuss the feasibility of these universal solid-state quantum gates, concluding that they are feasible with current technology.

PACS numbers: 03.67.Lx, 42.50.Ex, 42.50.Pq, 78.67.Hc

I. INTRODUCTION

Quantum logic gates are the key elements in quantum computing. It is well known that two-qubit entangling gates can be used to implement any n -qubit quantum computing, assisted by single-qubit gates [1, 2]. The family composed of controlled-NOT (CNOT) gates and one-qubit gates is the most popular universal set of quantum gates for quantum computing today [3–15]. The simulation of any two-qubit gate requires at least three CNOT gates and 15 single-qubit rotations [16–20]. Therefore, projects for realizing a CNOT gate in a solid-state system are highly desired for quantum computing in the future.

An optimal unstructured quantum circuit for any multi-qubit gate requires $\lceil \frac{1}{2}(4^n - 3n - 1) \rceil$ CNOT gates [19]. In the domain of a three-qubit case, people pay much attention to Toffoli [21] and Fredkin gates [22]. {Toffoli (Fredkin) gate, Hadamard gates} is a universal set for multi-qubit quantum computing [21, 22]. It is usual much more complex and difficult to realize a Toffoli gate or a Fredkin gate with CNOT and one-qubit gates in experiment because it requires at least six CNOT gates [23] to synthesize a Toffoli gate and it requires two CNOT and three controlled- $\sqrt{\text{NOT}}$ gates [24] to synthesize a Fredkin gate. It is particularly interesting to discuss the physical realization of a Toffoli gate and a Fredkin gate in a simpler way.

Quantum gates on solid-state systems have attracted much attention as they have a good scalability, and it has been demonstrated for superconducting qubits [25–27] and quantum dots [28]. Electron-spin qubits in solid-state systems, in particular, associated with nitrogen-vacancy (NV) defect centers, are particularly attractive.

The negatively charged NV defect center occurs in the

diamond lattice consisting of a substitutional ^{14}N atom and an adjacent vacancy, and is one of the most attracting and promising solid-state candidates for quantum information processing, due to the long room-temperature coherent time (1.8 *ms*) [29] that can be manipulated and coupled together in a scalable fashion. The procedures have been established for optical initialing, optical preparing, fast microwave or magnetic manipulating, and optical detecting the long-lived spin triplet state associated with NV centers [30–35].

Tremendous theoretical and experimental progress has been made on quantum information processing based on NV centers. The schemes for the quantum entanglement generation between a photon and an NV center [36], and between electrons associated with NV centers [37–41] were proposed. Recently, the schemes for the quantum state transfer between separated NV centers were introduced [42–44]. Multiqubit quantum registers associated with separated NV centers in diamonds have been proposed [37, 38, 42]. Hyperentanglement purification and concentration of two-photon systems in both the spatial-mode and polarization degrees of freedom were investigated [45] with the assistance of diamond NV centers inside photonic crystal cavities. Yang *et al.* [46] proposed a scheme for implementing the conditional phase gate between NV centers assisted by a high-Q silica microsphere cavity. As the electron spin of the NV defect center couples to nearby ^{13}C nuclear spins, a high-fidelity polarization and the detection of the single-electron and nuclear-spin states can be achieved, even under ambient conditions [47–50], which allows quantum information transfer [51–53], entanglement generation between an electron-spin qubit and a nuclear-spin qubit [54, 55] and between two nuclear spins [53], and the construction of the quantum gate between an electron and a nuclear spin [56].

In 2011, Chen *et al.* [39] proposed a composite system, i.e., a diamond NV^- center with six electrons from the nitrogen and three carbons surrounding the vacancy, which is confined in a microtoroidal resonator (MTR) [57]

*Published in Phys. Rev. A **88**, 042323 (2013)

[†]Corresponding author: fgdeng@bnu.edu.cn

with a quantized whispering-gallery mode (WGM). This system allows for an ultrahigh- Q and a small mode volume of WGM microresonators [58–60]. When the MTR couples to the fiber, the ultrahigh- Q is degraded. The experiments in which a diamond NV center couples to WGMs in a silica microsphere [61–63], diamond-GaP microdisk [64], or SiN photonic crystal [65] have been demonstrated. The photon input-output process of a coupled atom and MTR platform has been demonstrated in experiment [57].

It is important to construct compact quantum circuits for universal quantum gates because they reduce not only time but also errors. In this paper, we investigate the possibility of constructing compact universal quantum gates for a deterministic solid-state quantum computing, including the CNOT, Toffoli, and Fredkin gates on the diamond NV centers confined in cavities, by some single-photon input-output processes. The qubits of these deterministic gates are encoded on two of the electron-spin triple ground states associated with the diamond NV centers, and they have a long decoherence time even at the room temperature. Our quantum gates on NV centers are obtained by interacting a photon with the NV centers, detecting the emitting photon medium, and applying some proper feedforward operations on the electron-spin qubits associated with NV centers. Our quantum circuits for these gates are compact and economic. The CNOT and Toffoli gates are particularly appealed as the photon medium only interacts with each electron qubit one time. Compared with the synthesis programs, our schemes are simple. In our proposals, auxiliary electron-spin qubits are not required and only one photon medium is employed, which is different from the quantum gates on moving electrons based on charge detection [15] and the photonic quantum gates based on cross-Kerr nonlinearities [6]. With current technology, these universal solid-state quantum gates are feasible. If the photon loss, the detection inefficiency, and the imperfection of the experiment are negligible, the success probabilities of our gates are 100%.

This article is organized as follows. In Sec. II, we introduce the photon-matter platform based on the diamond NV center coupled to a resonator and the compact quantum circuit for a deterministic CNOT gate on two separated diamond NV centers. Subsequently, the quantum circuits for constructing three-qubit Toffoli and Fredkin gates on three separated diamond NV centers in a deterministic way are given in Secs. III and IV, respectively. The fidelities and efficiencies of our proposals are estimated in Sec. V. Finally, we discuss the feasibility of our universal quantum gates and give a summary in Sec. VI.

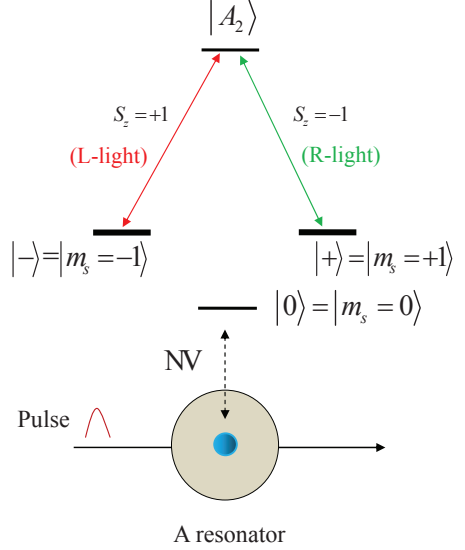


FIG. 1: (Color online) Schematic diagram of a diamond NV center coupling to a resonator and the possible Λ -type optical transitions in an NV center. The transition $|- \rangle \rightarrow |A_2 \rangle$ is derived by a left-circularly polarized photon (denoted by $|L \rangle$ or $S_z = +1$), and $|+ \rangle \rightarrow |A_2 \rangle$ is derived by a right-circularly polarized photon (denoted by $|R \rangle$ or $S_z = -1$). The levels in bold encode the qubits, i.e., $|+ \rangle = |m_s = +1 \rangle$ and $|- \rangle = |m_s = -1 \rangle$.

II. TWO-QUBIT CONTROLLED-NOT GATE ON AN NV-CENTER SYSTEM

A. A diamond NV center coupled to an MTR with a WGM

The electron-spin triple ground states of an NV center are split into $|m_s = 0 \rangle$ (denoted by $|0 \rangle$) and $|m_s = \pm 1 \rangle$ (denoted by $|\pm \rangle$) by 2.88 GHz with zero-field, due to the spin-spin interactions [66]. The structure of the excited states is relatively complex, and it includes six excited states defined by the method of group theory [36], $|A_1 \rangle = (|E_- \rangle|+ \rangle - |E_+ \rangle|- \rangle)/\sqrt{2}$, $|A_2 \rangle = (|E_- \rangle|+ \rangle + |E_+ \rangle|- \rangle)/\sqrt{2}$, $|E_x \rangle = |X \rangle|0 \rangle$, $|E_y \rangle = |Y \rangle|0 \rangle$, $|E_1 \rangle = (|E_- \rangle|- \rangle - |E_+ \rangle|+ \rangle)/\sqrt{2}$, and $|E_2 \rangle = (|E_- \rangle|- \rangle + |E_+ \rangle|+ \rangle)/\sqrt{2}$, owing to NV center's C_{3v} symmetry, spin-spin, and spin-orbit interactions in the absence of external magnetic field or crystal strain. Here, $|E_{\pm} \rangle$, $|X \rangle = (|E_- \rangle - |E_+ \rangle)/2$ and $|Y \rangle = i(|E_- \rangle + |E_+ \rangle)/2$ are the orbital states, and $|E_{\pm} \rangle$ has angular momentum projections ± 1 along the NV axis.

In our work, the quantum information of the quantum gate is encoded on the spins of the electronic ground triple states $|+ \rangle = |m_s = 1 \rangle$ and $|- \rangle = |m_s = -1 \rangle$. The Λ -type three-level system (see Fig.1) is realized by employing one of the specific excited state $|A_2 \rangle$ as an ancillary state [36]. The Λ -type system in which optical control is required, can be obtained by using a particular

magnetic field to mix the ground states [67]. Alternatively, it is possible to find a Λ -type system at zero magnetic field as the inevitable strain in diamond reduces the symmetry and primarily modifies the excited-state structure according to their orbital wave functions. The excited state is separated into two branches [68, 69], $|A_1\rangle$, $|A_2\rangle$, $|E_x\rangle$, and $|E_y\rangle$, $|E_1\rangle$, $|E_2\rangle$ at moderate and high strain. Togan *et al.* [36] demonstrated that the state $|A_2\rangle$ is robust to low strain and magnetic fields due to the stable symmetric properties, and it decays with an equal probability to the ground-state sublevels $|-\rangle$ through a left circularly polarized radiation $|L\rangle$ ($S_z = +1$) and to $|+\rangle$ through a right circularly polarized radiation $|R\rangle$ ($S_z = -1$). That is, the zero phonon line (ZPL) was observed after the optical resonant excitation at 637 nm ($|-\rangle \rightarrow |A_2\rangle$ driven by a L -polarized photon and $|+\rangle \rightarrow |A_2\rangle$ driven by a R -polarized photon). The mutually orthogonal circular polarization will be destroyed by high strain. The preparation and measurement of the electron spin can be realized by exploiting resonant optical excitation techniques. As illustrated in Ref. [36], the electron spin can be polarized by first preparing the electron spin to $|0\rangle$ by means of optical pumping with a 532-nm light, and then transferring the population to either $|\pm\rangle$ by means of microwave π pulses. The spin can be a high-fidelity ($\sim 93.2\%$) readout and addressed at low temperature ($T=8.6\text{K}$) based on spin-dependent optical transitions. The state $|A_2\rangle$ connects $|\pm 1\rangle$, and $|E_{x,y}\rangle$ connects $|0\rangle$, after spin manipulation by a microwave pulse and resonant excitation transition $|0\rangle \leftrightarrow |E_{x,y}\rangle$. The presence or absence of fluorescence decay reveals the spin state [36, 55].

The Heisenberg equations of the motion for the annihilation operator of the cavity mode \hat{a} and the lowering operator of the NV center operation σ_- and the input-output relation for the cavity are given by [70]

$$\begin{aligned}\frac{d\hat{a}}{dt} &= -\left[i(\omega_c - \omega_p) + \frac{\kappa}{2}\right]\hat{a}(t) - g\sigma_-(t) - \sqrt{\kappa}\hat{a}_{in}, \\ \frac{d\sigma_-}{dt} &= -\left[i(\omega_0 - \omega_p) + \frac{\gamma}{2}\right]\sigma_-(t) - g\sigma_z(t)\hat{a}(t) \\ &\quad + \sqrt{\gamma}\sigma_z(t)\hat{b}_{in}(t), \\ \hat{a}_{out} &= \hat{a}_{in} + \sqrt{\kappa}\hat{a}(t),\end{aligned}\quad (1)$$

where ω_c , ω_p , and ω_0 are the frequencies of the cavity, the single photon, and the NV center, respectively. $\hat{a}_{in}(t)$ and \hat{a}_{out} are the cavity input and output operators, respectively. $\sigma_z(t)$ is the inversion operator of the cavity. γ is the decay of the NV center. κ is the damping rate of the cavity. g is the coupling rate. $b_{in}(t)$ is the vacuum input field felt by the NV center with the commutation relation $[\hat{b}_{in}(t), \hat{b}_{in}^\dagger(t')] = \delta(t - t')$.

In a weak excitation, i.e., taking $\langle\sigma_z\rangle = -1$, the adiabatical elimination of the cavity mode leads to the reflection coefficient of the NV center confined in the cavity as

[71, 72]

$$r(\omega_p) = \frac{\hat{a}_{out}}{\hat{a}_{in}} = \frac{[i(\omega_c - \omega_p) - \frac{\kappa}{2}][i(\omega_0 - \omega_p) + \frac{\gamma}{2}] + g^2}{[i(\omega_c - \omega_p) + \frac{\kappa}{2}][i(\omega_0 - \omega_p) + \frac{\gamma}{2}] + g^2}. \quad (2)$$

The phase shift and the amplitude of the reflected photon are a function of the frequency detuning $\omega_c - \omega_p$, with $\omega_c = \omega_0$. For $\omega_c = \omega_0 = \omega_p$, i.e., when the cavity mode resonant with the NV center interacts with the resonant photon pulse, one can obtain [72]

$$r(\omega_p) = \frac{-\frac{\kappa\gamma}{4} + g^2}{\frac{\kappa\gamma}{4} + g^2}, \quad r_0(\omega_p) = -1. \quad (3)$$

Here, r_0 is the reflection coefficient of the cold (or the empty) cavity, that is, $g = 0$ and the cavity is not coupled to the NV center. $r(\omega_p)$ is the one for the hot cavity, i.e., $g \neq 0$. Therefore, the change of the input photon is summarized as [39]

$$\begin{aligned}|R\rangle|+\rangle &\rightarrow r|R\rangle|+\rangle, \\ |L\rangle|-\rangle &\rightarrow r|L\rangle|-\rangle, \\ |R\rangle|-\rangle &\rightarrow -|R\rangle|-\rangle, \\ |L\rangle|+\rangle &\rightarrow -|L\rangle|+\rangle.\end{aligned}\quad (4)$$

The effect of the coupling strength $g/\sqrt{\kappa\gamma}$ on the amplitude of the reflected photon and that of the frequency detuning on the phase shift have been discussed in [39]. Chen *et al.* [39] showed that when $g \geq 5\sqrt{\kappa\gamma}$ with $\omega_c = \omega_0 = \omega_p$,

$$r(\omega_p) \simeq 1, \quad r_0(\omega_p) = -1. \quad (5)$$

That is, Eq. (4) becomes

$$\begin{aligned}|R\rangle|+\rangle &\rightarrow |R\rangle|+\rangle, \\ |L\rangle|-\rangle &\rightarrow |L\rangle|-\rangle, \\ |R\rangle|-\rangle &\rightarrow -|R\rangle|-\rangle, \\ |L\rangle|+\rangle &\rightarrow -|L\rangle|+\rangle.\end{aligned}\quad (6)$$

From the Λ -type diamond NV-center optical transition depicted by Fig. 1, one can see that it requires a polarization-degenerate cavity mode. Therefore, it is suitable for not only WGM microresonators [38, 39, 57, 73], but also H1 photonic crystals [74, 75], micropillars [76–78], and fiber-based [79] cavities.

In our work, all the devices work under the resonant condition $\omega_c = \omega_0 = \omega_p$. In the following, we first consider the case $g \geq 5\sqrt{\kappa\gamma}$, that is, $r(\omega_p) \simeq 1$, and then we discuss the effect of $g/\sqrt{\kappa\gamma}$ on the fidelities and the efficiencies of our universal quantum gates on NV-center systems.

B. Compact quantum circuit for a two-qubit controlled-not gate on an NV-center system

Our quantum circuit for a CNOT gate on two NV centers is shown in Fig. 2. The two NV centers are initially prepared in two arbitrary superpositions of the two

ground states $|+\rangle$ and $|-\rangle$; that is,

$$\begin{aligned} |\psi\rangle_c^{el} &= \alpha_c|+\rangle_c + \beta_c|-\rangle_c, \\ |\psi\rangle_t^{el} &= \alpha_t|+\rangle_t + \beta_t|-\rangle_t. \end{aligned} \quad (7)$$

Here $|\alpha_c|^2 + |\beta_c|^2 = |\alpha_t|^2 + |\beta_t|^2 = 1$. The subscripts c and t stand for the control qubit NV_1 and the target qubit NV_2 , respectively. The single-photon medium is initially prepared in the equal superposition of $|R\rangle$ and $|L\rangle$; that is,

$$|\psi_0\rangle^{ph} = \frac{1}{\sqrt{2}}(|R\rangle + |L\rangle). \quad (8)$$

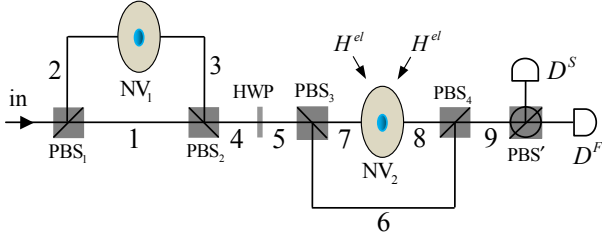


FIG. 2: (Color online) Compact quantum circuit for a CNOT gate on two NV centers. HWP is a half-wave plate set at 22.5° to complete the Hadamard operation (H^{ph}) on the polarization photon. The polarizing beam splitter PBS_i ($i = 1, 2$) in the basis $\{|R\rangle, |L\rangle\}$ transmits the right-circularly polarized photon $|R\rangle$ and reflects the left-circularly polarized photon $|L\rangle$, respectively. PBS' represents a PBS which transmits the photon in the state $|F\rangle = (|R\rangle + |L\rangle)/\sqrt{2}$ and reflects the photon in the state $|S\rangle = (|R\rangle - |L\rangle)/\sqrt{2}$, respectively. D^F and D^S are two single-photon detectors.

Polarizing beam splitter PBS_1 splits the input single photon into two wave-packets. The component $|R\rangle$ transmits through PBS_1 and then arrives at PBS_2 directly, while the component $|L\rangle$ is reflected to spatial mode 2 for interacting with NV_1 , which induces the transformation $|L\rangle_2(\alpha_c|+\rangle_c + \beta_c|-\rangle_c) \xrightarrow{NV_1} |L\rangle_3(-\alpha_c|+\rangle_c + \beta_c|-\rangle_c)$. Here and the after, the subscript i of $|L\rangle_i$ (or $|R\rangle_i$, $i = 1, 2, 3, \dots$) stands for the spatial mode i from where the L -polarized photon (R -polarized photon) emits. After the $|R\rangle_1$ and the $|L\rangle_3$ wave packets arrive at PBS_2 simultaneously, the photon emits from spatial mode 4. The specific evolution process of the whole system composed of the input photon and two NV centers can be

shown as follows:

$$\begin{aligned} |\Psi_0\rangle &= |\psi_0\rangle^{ph} \otimes |\psi\rangle_c^{el} \otimes |\psi\rangle_t^{el} \\ \xrightarrow{PBS_1} |\Psi_1\rangle &= \frac{1}{\sqrt{2}}(|R\rangle_1 + |L\rangle_2) \otimes |\psi\rangle_c^{el} \otimes |\psi\rangle_t^{el} \\ \xrightarrow{NV_1} |\Psi_2\rangle &= \frac{1}{\sqrt{2}}|R\rangle_1(\alpha_c|+\rangle_c + \beta_c|-\rangle_c) \otimes |\psi\rangle_t^{el} \\ &\quad + \frac{1}{\sqrt{2}}|L\rangle_3(-\alpha_c|+\rangle_c + \beta_c|-\rangle_c) \otimes |\psi\rangle_t^{el} \\ \xrightarrow{PBS_2} |\Psi_3\rangle &= \frac{1}{\sqrt{2}}|R\rangle_4(\alpha_c|+\rangle_c + \beta_c|-\rangle_c) \otimes |\psi\rangle_t^{el} \\ &\quad + \frac{1}{\sqrt{2}}|L\rangle_4(-\alpha_c|+\rangle_c + \beta_c|-\rangle_c) \otimes |\psi\rangle_t^{el}. \end{aligned} \quad (9)$$

From Eq. (9), one can see that the balanced Mach-Zehnder (MZ) interferometer composed of PBS_1 , NV_1 , and PBS_2 completes the operation

$$PBS_1 \rightarrow NV_1 \rightarrow PBS_2 = \begin{pmatrix} 1 & 0 & 0 & 0 \\ 0 & 1 & 0 & 0 \\ 0 & 0 & -1 & 0 \\ 0 & 0 & 0 & 1 \end{pmatrix}, \quad (10)$$

in the basis $\{|R\rangle|+\rangle, |R\rangle|-\rangle, |L\rangle|+\rangle, |L\rangle|-\rangle\}$.

Next, the photon passes through a half-wave plate HWP whose optical axes is set at 22.5° to complete the Hadamard gate (H^{ph}) on the polarization photon,

$$\begin{aligned} |R\rangle &\xrightarrow{H^{ph}} |F\rangle \equiv \frac{1}{\sqrt{2}}(|R\rangle + |L\rangle), \\ |L\rangle &\xrightarrow{H^{ph}} |S\rangle \equiv \frac{1}{\sqrt{2}}(|R\rangle - |L\rangle). \end{aligned} \quad (11)$$

That is, after an H^{ph} , the state of the whole system becomes

$$\begin{aligned} \xrightarrow{H^{ph}} |\Psi_4\rangle &= (\alpha_c|L\rangle_5|+\rangle_c + \beta_c|R\rangle_5|-\rangle_c) \\ &\quad \otimes (\alpha_t|+\rangle_t + \beta_t|-\rangle_t). \end{aligned} \quad (12)$$

PBS_3 transforms the wave packet $|L\rangle_5$ into $|L\rangle_6$, and transforms $|R\rangle_5$ into $|R\rangle_7$ for interacting with NV_2 and then it reaches PBS_4 simultaneously with $|L\rangle_6$. Before and after the photon passes through NV_2 , a Hadamard operation H^{el} is performed on NV_2 , respectively. According to Eq. (10), one can see that the above operations ($H^{el} \rightarrow PBS_3 \rightarrow NV_2 \rightarrow PBS_4 \rightarrow H^{el}$) complete the transformation as

$$\begin{aligned} \rightarrow |\Psi_5\rangle &= \alpha_c\alpha_t|L\rangle_9|+\rangle_c|+\rangle_t + \alpha_c\beta_t|L\rangle_9|+\rangle_c|-\rangle_t \\ &\quad + \beta_c\alpha_t|R\rangle_9|-\rangle_c|-\rangle_t + \beta_c\beta_t|R\rangle_9|-\rangle_c|+\rangle_t. \end{aligned} \quad (13)$$

Here Hadamard operation H^{el} completes the following transformations:

$$\begin{aligned} |+\rangle &\xrightarrow{H^{el}} |+\rangle \equiv \frac{1}{\sqrt{2}}(|+\rangle + |-\rangle), \\ |-\rangle &\xrightarrow{H^{el}} |-\rangle \equiv \frac{1}{\sqrt{2}}(|+\rangle - |-\rangle), \end{aligned} \quad (14)$$

From Eq. (13), one can see that to complete the CNOT gate on two NV centers, which implements the transformation

$$\begin{aligned} |\Psi\rangle_{ct} &= |\psi\rangle_c^e \otimes |\psi\rangle_t^e \\ &= \alpha_c |+\rangle_c (\alpha_t |+\rangle_t + \beta_t |-\rangle_t) \\ &\quad + \beta_c |-\rangle_c (\alpha_t |+\rangle_t + \beta_t |-\rangle_t), \\ &\xrightarrow{\text{CNOT}} \alpha_c |+\rangle_c (\alpha_t |+\rangle_t + \beta_t |-\rangle_t) \\ &\quad + \beta_c |-\rangle_c (\alpha_t |-\rangle_t + \beta_t |+\rangle_t), \end{aligned} \quad (15)$$

after the photon is detected by the detector D^F or D^S in the basis $\{|F\rangle = (|R\rangle + |L\rangle)/\sqrt{2}, |S\rangle = (|R\rangle - |L\rangle)/\sqrt{2}\}$, some proper single-qubit operations shown in Tab. I should be performed on the control qubit and the target qubit, respectively. Therefore, the quantum circuit shown in Fig. 2 performs the CNOT gate on two NV centers, which flips the state of the target electron qubit in NV_2 if and only if (iff) the control electron qubit in NV_1 is in the state $|-\rangle$. This gate works with a success probability of 100% in principle.

TABLE I: The feed-forward single unitary operations performed on the control and the target qubits correspond to the outcomes of the medium photon for completing the CNOT gate on the two NV centers with a success probability of 100%. $-\sigma_z = -|+\rangle\langle+| + |-\rangle\langle-|$. I_2 is a 2×2 unit operation which means doing nothing on a qubit.

photon	Feed-forward	
	control qubit	target qubit
$D^F (F\rangle)$	I_2	I_2
$D^S (S\rangle)$	$-\sigma_z$	I_2

III. SOLID-STATE TOFFOLI GATE ON A THREE-QUBIT NV-CENTER SYSTEM

A Toffoli gate is used to complete a NOT operation on the state of the target qubit when both two control qubits are in the state $|-\rangle$; otherwise, nothing is done on the target qubit. The principle for implementing a Toffoli gate on a three-qubit NV-center system is shown in Fig. 3. Suppose the first control qubit c_1 in the defect center NV_1 , the second control qubit c_2 in the defect center NV_2 , and the target qubit t in the defect center NV_3 are prepared in three arbitrary superposition electron-spin states as follows:

$$\begin{aligned} |\psi\rangle_{c_1}^e &= \alpha_{c_1} |+\rangle_{c_1} + \beta_{c_1} |-\rangle_{c_1}, \\ |\psi\rangle_{c_2}^e &= \alpha_{c_2} |+\rangle_{c_2} + \beta_{c_2} |-\rangle_{c_2}, \\ |\psi\rangle_t^e &= \alpha_t |+\rangle_t + \beta_t |-\rangle_t. \end{aligned} \quad (16)$$

Here, $|\alpha_{c_1}|^2 + |\beta_{c_1}|^2 = |\alpha_{c_2}|^2 + |\beta_{c_2}|^2 = |\alpha_t|^2 + |\beta_t|^2 = 1$.

In order to describe the principle of our Toffoli gate on a three-qubit NV-center system explicitly, we specify the evolution of the system as follows.

An input single-photon medium in the equal polarization superposition state $|\psi\rangle^{ph} = (|R\rangle + |L\rangle)/\sqrt{2}$ passes through a balanced MZ interferometer composed of PBS_1 , NV_1 , and PBS_2 described by Eq. (10), and then an H^{ph} (with HWP_1) is performed on it. PBS_3 transforms $|R\rangle_2$ into $|R\rangle_3$, and transforms $|L\rangle_2$ into $|L\rangle_4$. The evolution of the total states induced by the above operations ($PBS_1 \rightarrow NV_1 \rightarrow PBS_2 \rightarrow HWP_1 \rightarrow PBS_3$) can be described as follows:

$$\begin{aligned} |\Xi_0\rangle &= |\psi\rangle^{ph} \otimes |\psi\rangle_{c_1}^{el} \otimes |\psi\rangle_{c_2}^{el} \otimes |\psi\rangle_t^{el} \xrightarrow{PBS_1, NV_1, PBS_2} \\ |\Xi_1\rangle &= \frac{1}{\sqrt{2}} |R\rangle_1 (\alpha_{c_1} |+\rangle_{c_1} + \beta_{c_1} |-\rangle_{c_1}) \otimes |\psi\rangle_{c_2}^e \otimes |\psi\rangle_t^e \\ &\quad + \frac{1}{\sqrt{2}} |L\rangle_1 (-\alpha_{c_1} |+\rangle_{c_1} + \beta_{c_1} |-\rangle_{c_1}) \otimes |\psi\rangle_{c_2}^e \otimes |\psi\rangle_t^e \\ &\xrightarrow{HWP_1} |\Xi_2\rangle = (\alpha_{c_1} |L\rangle_2 |+\rangle_{c_1} + \beta_{c_1} |R\rangle_2 |-\rangle_{c_1}) \otimes |\psi\rangle_{c_2}^e \\ &\quad \otimes |\psi\rangle_t^e \\ &\xrightarrow{PBS_3} |\Xi_3\rangle = (\alpha_{c_1} |L\rangle_4 |+\rangle_{c_1} + \beta_{c_1} |R\rangle_3 |-\rangle_{c_1}) \otimes |\psi\rangle_{c_2}^e \\ &\quad \otimes |\psi\rangle_t^e. \end{aligned} \quad (17)$$

Before and after the photon emitting from spatial model 6 (5) passes through a balanced MZ interferometer composed of PBS_5 , NV_2 , and PBS_7 (PBS_4 , NV_2 , and PBS_6), an H^{ph} is performed on it, respectively. These processes ($HWP_3 \rightarrow PBS_5 \rightarrow NV_2 \rightarrow PBS_7 \rightarrow HWP_5$ and $HWP_2 \rightarrow PBS_4 \rightarrow NV_2 \rightarrow PBS_6 \rightarrow HWP_4$) complete the transformation $|\Xi_3\rangle \rightarrow |\Xi_4\rangle$. Here

$$\begin{aligned} |\Xi_4\rangle &= \alpha_{c_1} |+\rangle_{c_1} (\alpha_{c_2} |R\rangle_{10} |+\rangle_{c_2} + \beta_{c_2} |L\rangle_{10} |-\rangle_{c_2}) \otimes |\psi\rangle_t^e \\ &\quad + \beta_{c_1} |-\rangle_{c_1} (\alpha_{c_2} |R\rangle_9 |+\rangle_{c_2} + \beta_{c_2} |L\rangle_9 |-\rangle_{c_2}) \otimes |\psi\rangle_t^e. \end{aligned} \quad (18)$$

The transformation of $PBS_5 \rightarrow NV_2 \rightarrow PBS_7$ can be described by Eq. (10), and $PBS_4 \rightarrow NV_2 \rightarrow PBS_6$ can be written as

$$PBS_4 \rightarrow NV_2 \rightarrow PBS_6 = \begin{pmatrix} 1 & 0 & 0 & 0 \\ 0 & -1 & 0 & 0 \\ 0 & 0 & 1 & 0 \\ 0 & 0 & 0 & 1 \end{pmatrix}, \quad (19)$$

in the basis $\{|R\rangle|+\rangle, |R\rangle|-\rangle, |L\rangle|+\rangle, |L\rangle|-\rangle\}$. When the photon emits from spatial mode 10, it reaches the 50:50 BS directly. When the photon emits from spatial mode 9, before it reaches the 50:50 BS, it passes through a balanced MZ interferometer composed of PBS_8 , NV_3 , and PBS_9 described by Eq. (10), and an H^{el} is performed on the defect NV_3 before and after the photon transmits through it, respectively. The above operations ($H^{el} \rightarrow PBS_8 \rightarrow NV_3 \rightarrow PBS_9 \rightarrow H^{el}$) complete the transformation as

$$\begin{aligned} \rightarrow |\Xi_5\rangle &= \alpha_{c_1} \alpha_{c_2} |R\rangle_{10} |+\rangle_{c_1} |+\rangle_{c_2} (\alpha_t |+\rangle_t + \beta_t |-\rangle_t) \\ &\quad + \alpha_{c_1} \beta_{c_2} |L\rangle_{10} |+\rangle_{c_1} |-\rangle_{c_2} (\alpha_t |+\rangle_t + \beta_t |-\rangle_t) \\ &\quad + \beta_{c_1} \alpha_{c_2} |R\rangle_{11} |-\rangle_{c_1} |+\rangle_{c_2} (\alpha_t |+\rangle_t + \beta_t |-\rangle_t) \\ &\quad + \beta_{c_1} \beta_{c_2} |L\rangle_{11} |-\rangle_{c_1} |-\rangle_{c_2} (\alpha_t |-\rangle_t + \beta_t |+\rangle_t). \end{aligned} \quad (20)$$

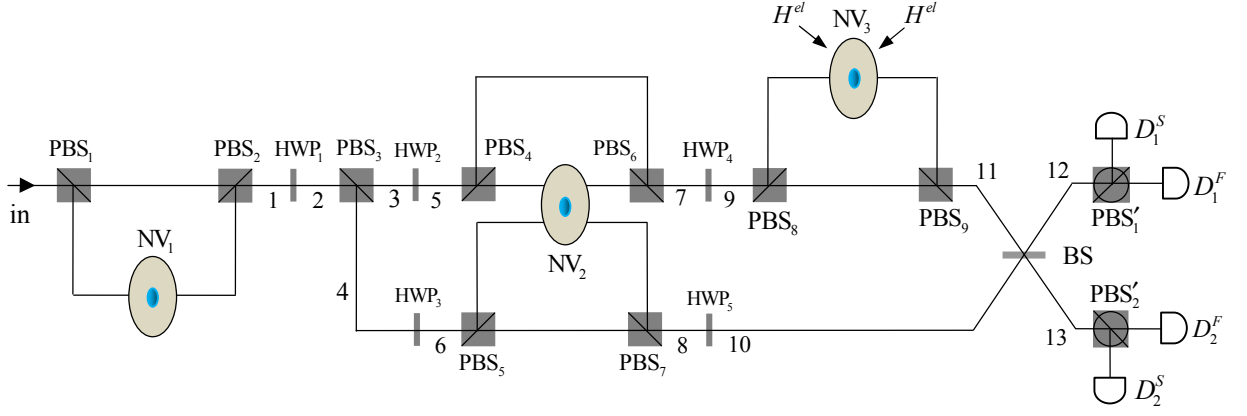


FIG. 3: (Color online) Compact quantum circuit for deterministically implementing a Toffoli gate on a quantum system composed of three NV centers.

Next, the wave packet emitting from spatial 11 interferes with the wave packet emitting from spatial 10 at the BS, which implements the transformations

$$\begin{aligned}
 |R\rangle_{11} &\xrightarrow{\text{BS}} \frac{1}{\sqrt{2}}(|R\rangle_{12} + |R\rangle_{13}), \\
 |L\rangle_{11} &\xrightarrow{\text{BS}} \frac{1}{\sqrt{2}}(|L\rangle_{12} + |L\rangle_{13}), \\
 |R\rangle_{10} &\xrightarrow{\text{BS}} \frac{1}{\sqrt{2}}(|R\rangle_{12} - |R\rangle_{13}), \\
 |L\rangle_{10} &\xrightarrow{\text{BS}} \frac{1}{\sqrt{2}}(|L\rangle_{12} - |L\rangle_{13}). \quad (21)
 \end{aligned}$$

$|\Xi\rangle_5$ will be transformed into the state

$$\begin{aligned}
 \xrightarrow{\text{BS}} |\Xi_6\rangle &= \frac{|F\rangle_{12}}{2} \left[\alpha_{c_1}\alpha_{c_2}|+\rangle_{c_1}|+\rangle_{c_2}(\alpha_t|+\rangle_t + \beta_t|-\rangle_t) + \alpha_{c_1}\beta_{c_2}|+\rangle_{c_1}|-\rangle_{c_2}(\alpha_t|+\rangle_t + \beta_t|-\rangle_t) \right. \\
 &\quad \left. + \beta_{c_1}\alpha_{c_2}|-\rangle_{c_1}|+\rangle_{c_2}(\alpha_t|+\rangle_t + \beta_t|-\rangle_t) + \beta_{c_1}\beta_{c_2}|-\rangle_{c_1}|-\rangle_{c_2}(\alpha_t|-\rangle_t + \beta_t|+\rangle_t) \right] \\
 &\quad + \frac{|S\rangle_{12}}{2} \left[\alpha_{c_1}\alpha_{c_2}|+\rangle_{c_1}|+\rangle_{c_2}(\alpha_t|+\rangle_t + \beta_t|-\rangle_t) - \alpha_{c_1}\beta_{c_2}|+\rangle_{c_1}|-\rangle_{c_2}(\alpha_t|+\rangle_t + \beta_t|-\rangle_t) \right. \\
 &\quad \left. + \beta_{c_1}\alpha_{c_2}|-\rangle_{c_1}|+\rangle_{c_2}(\alpha_t|+\rangle_t + \beta_t|-\rangle_t) - \beta_{c_1}\beta_{c_2}|-\rangle_{c_1}|-\rangle_{c_2}(\alpha_t|-\rangle_t + \beta_t|+\rangle_t) \right] \\
 &\quad + \frac{|F\rangle_{13}}{2} \left[-\alpha_{c_1}\alpha_{c_2}|+\rangle_{c_1}|+\rangle_{c_2}(\alpha_t|+\rangle_t + \beta_t|-\rangle_t) - \alpha_{c_1}\beta_{c_2}|+\rangle_{c_1}|-\rangle_{c_2}(\alpha_t|+\rangle_t + \beta_t|-\rangle_t) \right. \\
 &\quad \left. + \beta_{c_1}\alpha_{c_2}|-\rangle_{c_1}|+\rangle_{c_2}(\alpha_t|+\rangle_t + \beta_t|-\rangle_t) + \beta_{c_1}\beta_{c_2}|-\rangle_{c_1}|-\rangle_{c_2}(\alpha_t|-\rangle_t + \beta_t|+\rangle_t) \right] \\
 &\quad + \frac{|S\rangle_{13}}{2} \left[-\alpha_{c_1}\alpha_{c_2}|+\rangle_{c_1}|+\rangle_{c_2}(\alpha_t|+\rangle_t + \beta_t|-\rangle_t) + \alpha_{c_1}\beta_{c_2}|+\rangle_{c_1}|-\rangle_{c_2}(\alpha_t|+\rangle_t + \beta_t|-\rangle_t) \right. \\
 &\quad \left. + \beta_{c_1}\alpha_{c_2}|-\rangle_{c_1}|+\rangle_{c_2}(\alpha_t|+\rangle_t + \beta_t|-\rangle_t) - \beta_{c_1}\beta_{c_2}|-\rangle_{c_1}|-\rangle_{c_2}(\alpha_t|-\rangle_t + \beta_t|+\rangle_t) \right]. \quad (22)
 \end{aligned}$$

The photon medium is measured in the basis $\{|F\rangle, |S\rangle\}$ by the detector D_i^F or D_i^S . Following with the feedforward operations performed on the NV centers, shown in Table II, we accomplish the construction of the Tof-

foli gate on the three NV centers in a deterministic way. That is, the state of the system composed of the three

defect NV₁, NV₂, and NV₃ becomes

$$\begin{aligned} |\Xi\rangle_{\text{Toffoli}} = & \alpha_{c_1}\alpha_{c_2}|+\rangle_{c_1}|+\rangle_{c_2}(\alpha_t|+\rangle_t + \beta_t|-\rangle_t) \\ & + \alpha_{c_1}\beta_{c_2}|+\rangle_{c_1}|-\rangle_{c_2}(\alpha_t|+\rangle_t + \beta_t|-\rangle_t) \\ & + \beta_{c_1}\alpha_{c_2}|-\rangle_{c_1}|+\rangle_{c_2}(\alpha_t|+\rangle_t + \beta_t|-\rangle_t) \\ & + \beta_{c_1}\beta_{c_2}|-\rangle_{c_1}|-\rangle_{c_2}(\alpha_t|-\rangle_t + \beta_t|+\rangle_t). \end{aligned} \quad (23)$$

From the processes above, one can see that the setup shown in Fig. 3 completes the transformation,

$$\begin{aligned} |\Xi\rangle_{c_1, c_2, t} = & |\psi\rangle_{c_1}^{el} \otimes |\psi\rangle_{c_2}^{el} \otimes |\psi\rangle_t^{el} \\ \xrightarrow{\text{Toffoli}} & \alpha_{c_1}\alpha_{c_2}|+\rangle_{c_1}|+\rangle_{c_2}(\alpha_t|+\rangle_t + \beta_t|-\rangle_t) \\ & + \alpha_{c_1}\beta_{c_2}|+\rangle_{c_1}|-\rangle_{c_2}(\alpha_t|+\rangle_t + \beta_t|-\rangle_t) \\ & + \beta_{c_1}\alpha_{c_2}|-\rangle_{c_1}|+\rangle_{c_2}(\alpha_t|+\rangle_t + \beta_t|-\rangle_t) \\ & + \beta_{c_1}\beta_{c_2}|-\rangle_{c_1}|-\rangle_{c_2}(\alpha_t|-\rangle_t + \beta_t|+\rangle_t). \end{aligned} \quad (24)$$

That is, the setup shown in Fig. 3 realizes exactly the Toffoli gate on the three-qubit NV-center system, which flips the state of the target qubit iff both the two control qubits are in the state $|-\rangle$.

TABLE II: The operations performed on the control and the target qubits correspond to the measurement outcomes of the medium photon for completing the Toffoli gate on the three NV centers with a success probability of 100%.

photon	Feedforward		
	qubit c_1	qubit c_2	qubit t
$D_1^F (F\rangle_{12})$	I_2	I_2	I_2
$D_1^S (S\rangle_{12})$	I_2	σ_z	I_2
$D_2^F (F\rangle_{13})$	$-\sigma_z$	I_2	I_2
$D_2^S (S\rangle_{13})$	$-\sigma_z$	σ_z	I_2

IV. SOLID-STATE FREDKIN GATE ON A THREE-QUBIT NV-CENTER SYSTEM

A Fredkin gate is used to exchange the states of the two target qubits iff the control qubit is in the state $|-\rangle$. Our quantum circuit for implementing a Fredkin gate on a three-qubit NV-center system in a deterministic way is shown in Fig. 4. The control qubit c encoded on NV center “NV₁”, the first target qubit t_1 encoded on NV center “NV₂”, and the second target qubit t_2 encoded on NV center “NV₃” are initially prepared in three arbitrary states

$$\begin{aligned} |\psi\rangle_c^{el} &= \alpha_c|+\rangle_c + \beta_c|-\rangle_c, \\ |\psi\rangle_{t_1}^{el} &= \alpha_{t_1}|+\rangle_{t_1} + \beta_{t_1}|-\rangle_{t_1}, \\ |\psi\rangle_{t_2}^{el} &= \alpha_{t_2}|+\rangle_{t_2} + \beta_{t_2}|-\rangle_{t_2}. \end{aligned} \quad (25)$$

Here $|\alpha_c|^2 + |\beta_c|^2 = |\alpha_{t_1}|^2 + |\beta_{t_1}|^2 = |\alpha_{t_2}|^2 + |\beta_{t_2}|^2 = 1$. The photon medium p is prepared in the equal superposition state

$$|\psi\rangle^{ph} = \frac{1}{\sqrt{2}}(|R\rangle + |L\rangle). \quad (26)$$

That is, the initial state of the quantum system, composed of the three electrons c , t_1 , and t_2 , and a single photon p , can be written as

$$|\Pi_0\rangle = |\psi\rangle^{ph} \otimes |\psi\rangle_c^{el} \otimes |\psi\rangle_{t_1}^{el} \otimes |\psi\rangle_{t_2}^{el}. \quad (27)$$

In the following, let us discuss the construction of the solid-state Fredkin gate on a three-qubit NV-center system step by step.

First, a photon medium is injected into the input port *in* and it passes through a balanced MZ interferometer composed of PBS₁, NV₁, and PBS₂, and then an H^{ph} is performed on it (i.e., let it pass through HWP₁). PBS₃ transmits the R -polarized photon to spatial model 3, and reflects the L -polarized photon to spatial model 4. Based on the argument as made in Sec. III, one can see that the state of the whole system composed of a single photon medium and three NV centers then becomes

$$|\Pi_1\rangle = (\alpha_c|L\rangle_4|+\rangle_c + \beta_c|R\rangle_3|-\rangle_c) \otimes |\psi\rangle_{t_1}^e \otimes |\psi\rangle_{t_2}^e. \quad (28)$$

Before and after the photon emitting from spatial model 6 (5) passes through a balanced MZ interferometer composed of PBS₅, NV₂, NV₃, and PBS₇ (PBS₄, NV₂, NV₃, and PBS₆), an H^{ph} is performed on it, respectively. The state of the complicated system after these operations (HWP₃ \rightarrow PBS₅ \rightarrow NV₂ \rightarrow NV₃ \rightarrow PBS₇ \rightarrow HWP₅ and HWP₂ \rightarrow PBS₄ \rightarrow NV₂ \rightarrow NV₃ \rightarrow PBS₆ \rightarrow HWP₄) becomes

$$\begin{aligned} \rightarrow |\Pi_2\rangle = & \alpha_c\alpha_{t_1}\alpha_{t_2}|L\rangle_{10}|+\rangle_c|+\rangle_{t_1}|+\rangle_{t_2} \\ & - \alpha_c\alpha_{t_1}\beta_{t_2}|R\rangle_{10}|+\rangle_c|+\rangle_{t_1}|-\rangle_{t_2} \\ & - \alpha_c\beta_{t_1}\alpha_{t_2}|R\rangle_{10}|+\rangle_c|-\rangle_{t_1}|+\rangle_{t_2} \\ & + \alpha_c\beta_{t_1}\beta_{t_2}|L\rangle_{10}|+\rangle_c|-\rangle_{t_1}|-\rangle_{t_2} \\ & + \beta_c\alpha_{t_1}\alpha_{t_2}|R\rangle_9|-\rangle_c|+\rangle_{t_1}|+\rangle_{t_2} \\ & - \beta_c\alpha_{t_1}\beta_{t_2}|L\rangle_9|-\rangle_c|+\rangle_{t_1}|-\rangle_{t_2} \\ & - \beta_c\beta_{t_1}\alpha_{t_2}|L\rangle_9|-\rangle_c|-\rangle_{t_1}|+\rangle_{t_2} \\ & + \beta_c\beta_{t_1}\beta_{t_2}|R\rangle_9|-\rangle_c|-\rangle_{t_1}|-\rangle_{t_2}. \end{aligned} \quad (29)$$

Here the balanced MZ interferometer composed of PBS₅, NV₂, NV₃, and PBS₇ (PBS₄, NV₂, NV₃, and PBS₆) completes the unitary operation

$$\begin{aligned} \text{PBS}_{5(4)} \rightarrow \text{NV}_2 \rightarrow \text{NV}_3 \rightarrow \text{PBS}_{7(6)} \\ = \begin{pmatrix} 1 & 0 & 0 & 0 \\ 0 & -1 & 0 & 0 \\ 0 & 0 & -1 & 0 \\ 0 & 0 & 0 & I_5 \end{pmatrix}, \end{aligned} \quad (30)$$

in the basis $\{|R\rangle|+\rangle|+\rangle, |R\rangle|+\rangle|-\rangle, |R\rangle|-\rangle|+\rangle, |R\rangle|-\rangle|-\rangle, |L\rangle|+\rangle|+\rangle, |L\rangle|+\rangle|-\rangle, |L\rangle|-\rangle|+\rangle, |L\rangle|-\rangle|-\rangle\}$.

Next, when the photon emits from spatial mode 10, it reaches the 50:50 BS directly. When the photon emits from spatial mode 9, before it reaches the BS, it passes through a balanced MZ interferometer composed

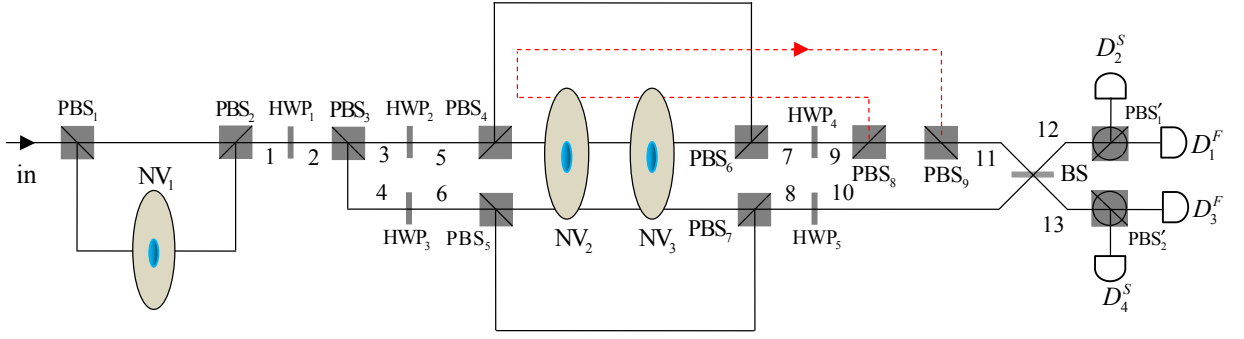


FIG. 4: (Color online) Schematic setup for deterministically implementing a Fredkin gate on three NV centers.

of PBS₈, PBS₉, NV₂ and NV₃, which completes the operation into

$$\text{PBS}_8 \rightarrow \text{NV}_3 \rightarrow \text{NV}_2 \rightarrow \text{PBS}_9 = \begin{pmatrix} I_5 & 0 & 0 & 0 \\ 0 & -1 & 0 & 0 \\ 0 & 0 & -1 & 0 \\ 0 & 0 & 0 & 1 \end{pmatrix}. \quad (31)$$

Before and after the photon interacts with NV₃ and NV₂, an H^{el} is performed on NV₃ and NV₂, respectively. These operations ($H^{el} \rightarrow \text{PBS}_8 \rightarrow \text{NV}_3 \rightarrow \text{NV}_2 \rightarrow \text{PBS}_9 \rightarrow H^{el}$) complete the transformation $|\Pi_2\rangle \rightarrow |\Pi_3\rangle$. Here

$$\begin{aligned} |\Pi_3\rangle = & \alpha_c \alpha_{t_1} \alpha_{t_2} |L\rangle_{10} |+\rangle_c |+\rangle_{t_1} |+\rangle_{t_2} \\ & - \alpha_c \alpha_{t_1} \beta_{t_2} |R\rangle_{10} |+\rangle_c |+\rangle_{t_1} |-\rangle_{t_2} \\ & - \alpha_c \beta_{t_1} \alpha_{t_2} |R\rangle_{10} |+\rangle_c |-\rangle_{t_1} |+\rangle_{t_2} \\ & + \alpha_c \beta_{t_1} \beta_{t_2} |L\rangle_{10} |+\rangle_c |-\rangle_{t_1} |-\rangle_{t_2} \\ & + \beta_c \alpha_{t_1} \alpha_{t_2} |R\rangle_{11} |-\rangle_c |+\rangle_{t_1} |+\rangle_{t_2} \\ & - \beta_c \alpha_{t_1} \beta_{t_2} |L\rangle_{11} |-\rangle_c |+\rangle_{t_1} |+\rangle_{t_2} \\ & - \beta_c \beta_{t_1} \alpha_{t_2} |L\rangle_{11} |-\rangle_c |+\rangle_{t_1} |-\rangle_{t_2} \\ & + \beta_c \beta_{t_1} \beta_{t_2} |R\rangle_{11} |-\rangle_c |+\rangle_{t_1} |-\rangle_{t_2}. \end{aligned} \quad (32)$$

The 50:50 BS, described by Eq. (21), transforms $|\Pi_3\rangle$

$$\begin{aligned} |\Pi_4\rangle = & \frac{|F_{12}\rangle}{2} \left[\alpha_c |+\rangle_c (\alpha_{t_1} |+\rangle_{t_1} - \beta_{t_1} |-\rangle_{t_1}) \right. \\ & \times (\alpha_{t_2} |+\rangle_{t_2} - \beta_{t_2} |-\rangle_{t_2}) + \beta_c |-\rangle_c (\alpha_{t_2} |+\rangle_{t_1} \\ & - \beta_{t_2} |-\rangle_{t_1}) (\alpha_{t_1} |+\rangle_{t_2} - \beta_{t_1} |-\rangle_{t_2}) \Big] \\ & + \frac{|S_{12}\rangle}{2} \left[-\alpha_c |+\rangle_c (\alpha_{t_1} |+\rangle_{t_1} + \beta_{t_1} |-\rangle_{t_1}) \right. \\ & \times (\alpha_{t_2} |+\rangle_{t_2} + \beta_{t_2} |-\rangle_{t_2}) + \beta_c |-\rangle_c (\alpha_{t_2} |+\rangle_{t_1} \\ & + \beta_{t_2} |-\rangle_{t_1}) (\alpha_{t_1} |+\rangle_{t_2} + \beta_{t_1} |-\rangle_{t_2}) \Big] \\ & + \frac{|F_{13}\rangle}{2} \left[-\alpha_c |+\rangle_c (\alpha_{t_1} |+\rangle_{t_1} - \beta_{t_1} |-\rangle_{t_1}) \right. \\ & \times (\alpha_{t_2} |+\rangle_{t_2} - \beta_{t_2} |-\rangle_{t_2}) + \beta_c |-\rangle_c (\alpha_{t_2} |+\rangle_{t_1} \\ & - \beta_{t_2} |-\rangle_{t_1}) (\alpha_{t_1} |+\rangle_{t_2} - \beta_{t_1} |-\rangle_{t_2}) \Big] \\ & + \frac{|S_{13}\rangle}{2} \left[\alpha_c |+\rangle_c (\alpha_{t_1} |+\rangle_{t_1} + \beta_{t_1} |-\rangle_{t_1}) \right. \\ & \times (\alpha_{t_2} |+\rangle_{t_2} + \beta_{t_2} |-\rangle_{t_2}) + \beta_c |-\rangle_c (\alpha_{t_2} |+\rangle_{t_1} \\ & + \beta_{t_2} |-\rangle_{t_1}) (\alpha_{t_1} |+\rangle_{t_2} + \beta_{t_1} |-\rangle_{t_2}) \Big]. \end{aligned} \quad (33)$$

Third, by detecting the single-photon medium in the basis $\{|F\rangle, |S\rangle\}$ and following with the feedforward single-qubit unitary operations shown in Table III, one can see that the state of the system composed of NV₁, NV₂, and NV₃ becomes

$$\begin{aligned} |\Pi\rangle_{\text{Fredkin}} = & \alpha_c |+\rangle_c (\alpha_{t_1} |+\rangle_{t_1} + \beta_{t_1} |-\rangle_{t_1}) \\ & \times (\alpha_{t_2} |+\rangle_{t_2} + \beta_{t_2} |-\rangle_{t_2}) \\ & + \beta_c |-\rangle_c (\alpha_{t_2} |+\rangle_{t_1} + \beta_{t_2} |-\rangle_{t_1}) \\ & \times (\alpha_{t_1} |+\rangle_{t_2} + \beta_{t_1} |-\rangle_{t_2}). \end{aligned} \quad (34)$$

Comparing Eq. (28) with Eq. (34), one can see that the quantum circuit shown in Fig. 4 implements a Fredkin gate on the three NV centers with the success probability of 100% in principle, which swaps the states of two target qubits iff the control qubit is in the state $|-\rangle$.

TABLE III: The operations performed on the control and the target qubits correspond to the measurement outcomes of the medium photon for completing the Fredkin gate on the three NV centers with a success probability of 100%.

photon	Feedforward		
	qubit c	qubit t_1	qubit t_2
$D_1^F(F\rangle_{12})$	I_2	σ_z	σ_z
$D_1^S(S\rangle_{12})$	$-\sigma_z$	I_2	I_2
$D_2^F(F\rangle_{13})$	$-\sigma_z$	σ_z	σ_z
$D_2^S(S\rangle_{13})$	I_2	I_2	I_2

V. FIDELITIES AND EFFICIENCIES OF OUR UNIVERSAL QUANTUM GATES

Let us estimate the fidelities and the efficiencies of our universal solid-state quantum gates discussed above, defining the fidelity as $F = |\langle \psi_{\text{real}} | \psi_{\text{ideal}} \rangle|^2$. Here, $|\psi_{\text{ideal}}\rangle$ is the target state of the NV-center-cavity system encoded for the quantum gate in the ideal case $g \geq 5\sqrt{\kappa\gamma}$, and $|\psi_{\text{real}}\rangle$ is the target state of a realistic NV-center-cavity system. Defining the efficiency as the yield of the photons, that is, $\eta = n_{\text{output}}/n_{\text{input}}$. Here, n_{input} is the number of the input photon, whereas n_{output} is the number of the output photon. The gates are realized by the input-output processes of the photon medium, which means that the reflection coefficient of the NV-cavity system determines the fidelities and the efficiencies of our universal quantum gates.

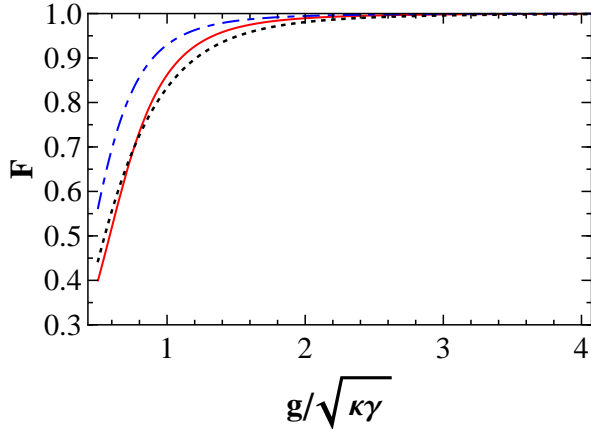


FIG. 5: (Color online) The fidelities of the CNOT (solid line, red), Toffoli (dash-dotted line, blue), and Fredkin (dotted line, black) gates vs $g/\sqrt{\kappa\gamma}$. Here, $g/\sqrt{\kappa\gamma} \geq 0.5$.

Combing the specific evolutions of the CNOT, Toffoli, and Fredkin gates and the input-output relations of the NV-cavity system in the realistic case given by Eq. (4), one can see that the fidelities of those gates can be cal-

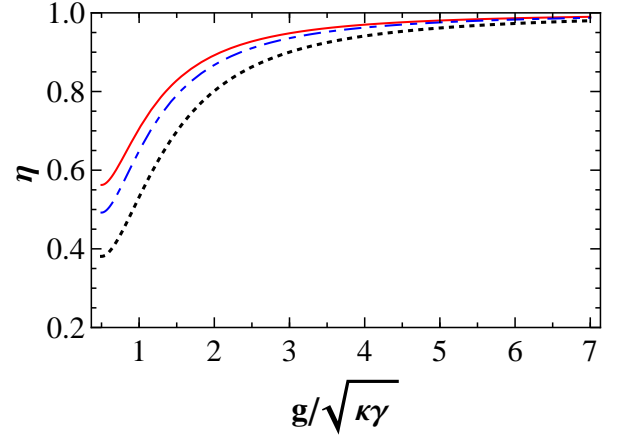


FIG. 6: (Color online) The efficiencies of the CNOT (solid line, red), Toffoli (the dash-dotted line, blue), and Fredkin (dotted line, black) gates vs $g/\sqrt{\kappa\gamma}$. Here, $g/\sqrt{\kappa\gamma} \geq 0.5$.

culated as

$$\begin{aligned}
 F_{\text{CNOT}} &= \frac{(2 + |r| + |r|^2)^2}{2(5 - 2|r| + 2|r|^2 + 2|r|^3 + |r|^4)}, \\
 F_{\text{Toffoli}} &= \frac{(3 + |r|)^4}{16(3 + |r|^2)^2}, \\
 F_{\text{Fredkin}} &= \frac{\zeta_{\text{Fredkin}}}{\xi_{\text{Fredkin}}},
 \end{aligned} \tag{35}$$

with

$$\begin{aligned}
 \zeta_{\text{Fredkin}} &= (29 + 19|r| + 8|r|^2 + 4|r|^3 + 3|r|^4 + |r|^5)^2, \\
 \xi_{\text{Fredkin}} &= 8[237 - 10|r| + 165|r|^2 - 8|r|^3 + 66|r|^4 \\
 &\quad - 12|r|^5 + 26|r|^6 + |r|^7(3 + |r|) \\
 &\quad \times (8 + 3|r| + |r|^2)].
 \end{aligned} \tag{36}$$

The efficiencies of those gates can be calculated as

$$\begin{aligned}
 \eta_{\text{CNOT}} &= \left[\frac{3 + |r|^2}{4} \right]^2, \\
 \eta_{\text{Toffoli}} &= \frac{(3 + |r|^2)^2(7 + |r|^2)}{128}, \\
 \eta_{\text{Fredkin}} &= \frac{(3 + |r|^2)[4 + (1 + |r|^2)^2][12 + (1 + |r|^2)^2]}{512}.
 \end{aligned} \tag{37}$$

For the diamond NV centers, the photoluminescence is partially unpolarized, and the emission with ZPL is only 4% of the total emission. γ_{ZPL} with zero phonon line is only 4% of $\gamma_{\text{total}} = 2\pi \times 15$ MHz [36, 66]. $Q = c/\lambda\kappa$, where c is the speed of light and $\lambda = 637$ nm is the transition wavelength. The WGM cavities with microtoroidal form have attracted much attention [80]. Ref. [80] shows that the polymer-coated microtoroid is feasible and robust in experiments. For the diamond NV center in a MTR with WGM mode system, Ref. [36] shows that

when $g/\sqrt{\kappa\gamma} \geq 3$ with $\omega_c = \omega_p = \omega_0$, $r(\omega_p) \sim 0.95$; when $g/\sqrt{\kappa\gamma} \geq 5$ with $\omega_c = \omega_p = \omega_0$, $Q \sim 10^5$ (corresponding to $\kappa \sim 1$ GHz) or $Q \sim 10^4$ (corresponding to $\kappa \sim 10$ GHz), $r(\omega_p) \sim 1$.

Figures 5 and 6 show the fidelities and the efficiencies of our universal quantum gates as a function of $g/\sqrt{\kappa\gamma}$ with $\omega_c = \omega_p = \omega_0$ and $g/\sqrt{\kappa\gamma} \geq 1/2$. Our results show that the fidelities and the efficiencies of our quantum gates increase with $g/\sqrt{\kappa\gamma}$. When $g/\sqrt{\kappa\gamma} = 5$, the fidelities of the gates are unity with $\eta_{\text{CNOT}} = 98.05\%$, $\eta_{\text{Toffoli}} = 97.57\%$, and $\eta_{\text{Fredkin}} = 96.15\%$.

VI. DISCUSSION AND SUMMARY

Universal quantum gates in solid-state systems are much more attractive as they have a good scalability. Many schemes have been proposed for realizing universal quantum gates on solid-state systems. Based on superconductor, Romero *et al.* [25] and Stojanović *et al.* [26] proposed some interesting schemes for realizing controlled-phase and Toffoli gates in nanosecond time scale, respectively. Liang and Li [81] proposed a scheme for realizing a SWAP gate between the flying and the stationary qubits. In 2010, the quantum circuit for realizing a CNOT between a quantum-dot qubit and a polarized photon qubit was designed by Bonato *et al.* [13]. Based on appealing diamond NV-center qubits, Yang *et al.* [46] proposed a scheme for realizing a conditional phase gate between NV centers assisted by high-Q silica microsphere cavity, and the control and the target qubits are encoded on different energy levels. Jelezko *et al.* [56] designed a quantum circuit for realizing controlled-ROT gate between an electron and a nuclear spin qubits in a NV center.

The schemes we proposed for constructing the two-qubit CNOT, and three-qubit Toffoli and Fredkin gates on diamond NV centers inside resonators have some interesting features. (1) The quantum circuits are compact. Especially the schemes for CNOT and Toffoli gates, in which the photon medium only interacts with each qubit one time. The complexity of our schemes for Toffoli and Fredkin gates beats its synthesis procedure. The optimal synthesis of a Toffoli [23] gates requires six CNOT gates. A Fredkin gate can be decomposed into six specific gates [24], i.e., two CNOT and three controlled- $\sqrt{\text{NOT}}$ gates. (2) Our schemes are economic. Auxiliary electron qubits are employed in Refs. [15, 82], but they are not

required in our schemes. Furthermore, only one single-photon medium is employed in our proposals. (3) The static electron qubits employed in our proposals are more robust than the moving qubits in Ref. [15]. (4) Different from Refs. [13, 56, 81] (the hybrid qubits are employed), all the qubits in our proposals are encoded on the spins of the electrons associated with NV centers, which means our quantum gates are scalable. Unfortunately, identical NV centers are required in our proposals, although the identical NV centers are challenge with current techniques, the energy levels of different NV centers can be adjusted by external magnetic fields. (5) They have a long coherence time in NV centers even at the room temperature. (6) Different from Ref. [46], all of the qubits in our proposals are encoded on the identical energy levels. (7) Our proposals are robust against low strain and magnetic fields, due to the special auxiliary energy level we employed. (8) Compared with an atom-cavity system, the time scale for manipulating an NV center is much shorter than that seen with an atom. Also it is difficult to trapped an atom in the cavity. Although high fidelities and efficiencies can be achieved in our schemes, only 4% of the emitted photon emitting from the NV centers are coherent emissions within the narrowband ZPL at 637 nm due to the particular characteristic of the NV centers.

In summary, we have designed the compact quantum circuits for implementing some deterministic universal quantum gates on NV centers, including the CNOT, Toffoli, and Fredkin gates, by means of the interaction between an NV-cavity-assisted qubit and a single-photon medium in a scalable fashion. The quantum gates are constructed by some input-output processes of a single photon medium, the measurements on the polarizations of the photon medium, and feedforward operations. As these quantum gates have a long coherence time even at the room temperature and they are universal, intrinsically deterministic, and scalable, they provide a different way for quantum computing in solid-state quantum systems.

ACKNOWLEDGEMENTS

This work is supported by the National Natural Science Foundation of China under Grant No. 11174039 and NECT-11-0031

-
- [1] M. A. Nielsen and I. L. Chuang, *Quantum Computation and Quantum Information* (Cambridge University Press, Cambridge, 2000).
 - [2] A. Barenco, C. H. Bennett, R. Cleve, D. P. DiVincenzo, N. Margolus, P. Shor, T. Sleator, J. A. Smolin, and H. Weinfurter, Phys. Rev. A **52**, 3457 (1995).

- [3] E. Knill, R. Laflamme, and G. J. Milburn, Nature (London) **409**, 46 (2001).
- [4] J. L. O'Brien, G. J. Pryde, A. G. White, T. C. Ralph, and D. Branning, Nature (London) **426**, 264 (2003).
- [5] M. A. Nielsen, Phys. Rev. Lett. **93**, 040503 (2004).
- [6] K. Nemoto and W. J. Munro, Phys. Rev. Lett. **93**, 250502 (2004).

- (2004).
- [7] D. E. Browne and T. Rudolph, *Phys. Rev. Lett.* **95**, 010501 (2005).
 - [8] H. R. Wei and F. G. Deng, *Opt. Express* **21**, 17671 (2013).
 - [9] B. C. Ren, H. R. Wei and F. G. Deng, *Laser Phys. Lett.* **10**, 095202 (2013).
 - [10] G. L. Long and L. Xiao, *Phys. Rev. A* **69**, 052303 (2004).
 - [11] G. Feng, G. Xu, and G. Long, *Phys. Rev. Lett.* **110**, 190501 (2013).
 - [12] C. Y. Hu, W. J. Munro, J. L. O'Brien, and J. G. Rarity, *Phys. Rev. B* **80**, 205326 (2009).
 - [13] C. Bonato, F. Haupt, S. S. R. Oemrawsingh, J. Gudat, D. Ding, M. P. van Exter, and D. Bouwmeester, *Phys. Rev. Lett.* **104**, 160503 (2010).
 - [14] H. R. Wei and F. G. Deng, *Phys. Rev. A* **87**, 022305 (2013).
 - [15] C. W. J. Beenakker, D. P. DiVincenzo, C. Emary, and M. Kindermann, *Phys. Rev. Lett.* **93**, 020501 (2004).
 - [16] G. Vidal and C. M. Dawson, *Phys. Rev. A* **69**, 010301 (2004).
 - [17] F. Vatan and C. Williams, *Phys. Rev. A* **69**, 032315 (2004).
 - [18] J. Zhang, J. Vala, S. Sastry, and K. B. Whaley, *Phys. Rev. A* **69**, 042309 (2004).
 - [19] V. V. Shende, I. L. Markov, and S. S. Bullock, *Phys. Rev. A* **69**, 062321 (2004).
 - [20] V. V. Shende, S. S. Bullock, and I. L. Markov, *Phys. Rev. A* **70**, 012310 (2004).
 - [21] Y. Y. Shi, *Quantum Inf. Comput.* **3**, 84 (2003).
 - [22] E. Fredkin and T. Toffoli, *Int. J. Theor. Phys.* **21**, 219 (1982).
 - [23] V. V. Shende and I. L. Markov, *Quant. Inf. Comput.* **9**, 461 (2009).
 - [24] J. A. Smolin and D. P. DiVincenzo, *Phys. Rev. A* **53**, 2855 (1996).
 - [25] G. Romero, D. Ballester, Y. M. Wang, V. Scarani, and E. Solano, *Phys. Rev. Lett.* **108**, 120501 (2012).
 - [26] V. M. Stojanović, A. Fedorov, A. Wallraff, and C. Bruder, *Phys. Rev. B* **85**, 054504 (2012).
 - [27] T. Yamamoto, Y. A. Pashkin, O. Astafiev, Y. Nakamura, and J. S. Tsai, *Nature (London)* **425**, 941 (2003).
 - [28] X. Q. Li, Y. W. Wu, D. Steel, D. Gammon, T. H. Stievater, D. S. Katzer, D. Park, C. Piermarocchi, and L. J. Sham, *Science* **301**, 809 (2003).
 - [29] G. Balasubramanian, P. Neumann, D. Twitchen, M. Markham, R. Kolesov, N. Mizuochi, J. Isoya, J. Achard, J. Beck, J. Tessler, V. Jacques, P. R. Hemmer, F. Jelezko, and J. Wrachtrup, *Nature Mater.* **8**, 383 (2009).
 - [30] F. Jelezko, T. Gaebel, I. Popa, A. Gruber, and J. Wrachtrup, *Phys. Rev. Lett.* **92**, 076401 (2004).
 - [31] T. Gaebel, M. Domhan, I. Popa, C. Wittmann, P. Neumann, F. Jelezko, J. R. Rabreau, N. Stavrias, A. D. Greentree, S. Praver, J. Meijer, J. Twamley, P. R. Hemmer, and J. Wrachtrup, *Nature Phys.* **2**, 408 (2006).
 - [32] R. Hanson, F. M. Mendoza, R. J. Epstein, and D. D. Awschalom, *Phys. Rev. Lett.* **97**, 087601 (2006).
 - [33] R. J. Epstein, F. M. Mendoza, Y. K. Kato, and D. D. Awschalom, *Nature Phys.* **1**, 94 (2005).
 - [34] G. D. Fuchs, V. V. Dobrovitski, D. M. Toyli, F. J. Heremans, and D. D. Awschalom, *Science* **326**, 1520 (2009).
 - [35] F. T. Charnock and T. A. Kennedy, *Phys. Rev. B* **64**, 041201 (2001).
 - [36] E. Togan, Y. Chu, A. S. Trifonov, L. Jiang, J. Maze, L. Childress, M. V. G. Dutt, A. S. Sørensen, P. R. Hemmer, A. S. Zibrov, and M. D. Lukin, *Nature (London)* **466**, 730 (2010).
 - [37] P. Neumann, R. Kolesov, B. Naydenov, J. Beck, F. Rempp, M. Steiner, V. Jacques, G. Balasubramanian, M. L. Markham, D. J. Twitchen, S. Pezzagna, J. Meijer, J. Twamley, F. Jelezko, and J. Wrachtrup, *Nature Phys.* **6**, 249 (2010).
 - [38] W. L. Yang, Z. Y. Xu, M. Feng, and J. F. Du, *New J. Phys.* **12**, 113039 (2010).
 - [39] Q. Chen, W. L. Yang, M. Feng, and J. F. Du, *Phys. Rev. A* **83**, 054305 (2011).
 - [40] A. S. Zheng, J. H. Li, R. Yu, X. Y. Lü, and Y. Wu, *Opt. Express* **20**, 16902 (2012).
 - [41] Z. Y. Xu, Y. M. Hu, W. L. Yang, M. Feng, and J. F. Du, *Phys. Rev. A* **80**, 022335 (2009).
 - [42] Y. J. Zhao, X. M. Fang, F. Zhou, and K. H. Song, *Phys. Rev. A* **86**, 052325 (2012).
 - [43] P. B. Li, S. Y. Gao, and F. L. Li, *Phys. Rev. A* **83**, 054306 (2011).
 - [44] W. L. Yang, Z. Q. Yin, Z. Y. Xu, M. Feng, and C. H. Oh, *Phys. Rev. A* **84**, 043849 (2011).
 - [45] B. C. Ren and F. G. Deng, *Laser Phys. Lett.* **10**, 115201 (2013).
 - [46] W. L. Yang, Z. Q. Yin, Z. Y. Xu, M. Feng, and J. F. Du, *Appl. Phys. Lett.* **96**, 241113 (2010).
 - [47] A. Beveratos, R. Brouri, T. Gacoin, J. P. Poizat, and P. Grangier, *Phys. Rev. A* **64**, 061802 (2001).
 - [48] C. Kurtsiefer, S. Mayer, P. Zarda, and H. Weinfurter, *Phys. Rev. Lett.* **85**, 290 (2000).
 - [49] A. Gruber, A. Dräbenstedt, C. Tietz, L. Fleury, J. Wrachtrup, and C. von Borczyskowski, *Science* **276**, 2012 (1997).
 - [50] L. Childress, M. V. G. Dutt, J. M. Taylor, A. S. Zibrov, F. Jelezko, J. Wrachtrup, P. R. Hemmer, and M. D. Lukin, *Science* **314**, 281 (2006).
 - [51] M. V. G. Dutt, L. Childress, L. Jiang, E. Togan, J. Maze, F. Jelezko, A. S. Zibrov, P. R. Hemmer, and M. D. Lukin, *Science* **316**, 1312 (2007).
 - [52] G. D. Fuchs, G. Burkard, P. V. Klimov, and D. D. Awschalom, *Nature Phys.* **7**, 789 (2011).
 - [53] P. Neumann, N. Mizuochi, F. Rempp, P. Hemmer, H. Watanabe, S. Yamasaki, V. Jacques, T. Gaebel, F. Jelezko, and J. Wrachtrup, *Science* **320**, 1326 (2008).
 - [54] M. Mehring, J. Mende, and W. Scherer, *Phys. Rev. Lett.* **90**, 153001 (2003).
 - [55] L. Robledo, L. Childress, H. Bernien, B. Hensen, P. F. A. Alkemade, and R. Hanson, *Nature (London)* **477**, 574 (2011).
 - [56] F. Jelezko, T. Gaebel, I. Popa, M. Domhan, A. Gruber, and J. Wrachtrup, *Phys. Rev. Lett.* **93**, 130501 (2004).
 - [57] B. Dayan, A. S. Parkins, T. Aoki, E. P. Ostby, K. J. Vahala, and H. J. Kimble, *Science* **319**, 1062 (2008).
 - [58] S. M. Spillane, T. J. Kippenberg, K. J. Vahala, K. W. Goh, E. Wilcut, and H. J. Kimble, *Phys. Rev. A* **71**, 013817 (2005).
 - [59] Y. Louyer, D. Meschede, and A. Rauschenbeutel, *Phys. Rev. A* **72**, 031801 (2005).
 - [60] K. J. Vahala, *Nature (London)* **424**, 839 (2003).
 - [61] Y. S. Park, A. K. Cook, and H. Wang, *Nano. Lett.* **6**, 2075 (2006).
 - [62] M. Larsson, K. N. Dinyari, and H. Wang, *Nano. Lett.* **9**, 1447 (2009).
 - [63] R. J. Barbour, K. N. Dinyari, and H. Wang, *Opt. Express*

- 18**, 18968 (2010).
- [64] P. E. Barclay, K. M. C. Fu, C. Santori, and R. G. Beausoleil, *Appl. Phys. Lett.* **95**, 191115 (2009).
 - [65] M. W. McCutcheon and M. Lončar, *Opt. Express* **16**, 19136 (2008).
 - [66] N. B. Manson, J. P. Harrison, and M. J. Sellars, *Phys. Rev. B* **74**, 104303 (2006).
 - [67] P. R. Hemmer, A. V. Turukhin and M. S. Shahriar, J. A. Musser, *Optics Lett.* **26**, 361 (2001).
 - [68] C. Santori, P. Tamarat, P. Neumann, J. Wrachtrup, D. Fattal, R. G. Beausoleil, *Phys. Rev. Lett.* **97**, 247401 (2006).
 - [69] C. Santori, D. Fattal, S. M. Spillane, et al., *Opt. Express* **14**, 7986 (2006).
 - [70] D. F. Walls and G. J. Milburn, *Quantum Optics* (Springer-Verlag, Berlin, 1994).
 - [71] C. Y. Hu, A. Young, J. L. O'Brien, W. J. Munro, and J. G. Rarity, *Phys. Rev. B* **78**, 085307 (2008).
 - [72] J. H. An, M. Feng, and C. H. Oh, *Phys. Rev. A* **79**, 032303 (2009).
 - [73] J. T. Shen and S. Fan, *Phys. Rev. A* **82**, 021802 (2010).
 - [74] I. J. Luxmoore, E. D. Ahmadi, B. J. Luxmoore, N. A. Wasley, A. I. Tartakovskii, M. Hugues, M. S. Skolnick, and A. M. Fox, *Appl. Phys. Lett.* **100**, 121116 (2012).
 - [75] J. Hagemeyer, C. Bonato, T. A. Truong, H. Kim, G. J. Beirne, M. Bakker, M. P. van Exter, Y. Q. Luo, P. Petroff, and D. Bouwmeester, *Opt. Express* **20**, 24714 (2012).
 - [76] C. Bonato, D. Ding, J. Gudat, S. Thon, H. Kim, P. M. Petroff, M. P. van Exter, and D. Bouwmeester, *Appl. Phys. Lett.* **95**, 251104 (2009).
 - [77] J. Gudat, C. Bonato, E. van Nieuwenburg, S. Thon, H. Kim, P. M. Petroff, M. P. van Exter, and D. Bouwmeester, *Appl. Phys. Lett.* **98**, 121111 (2011).
 - [78] C. Bonato, E. van Nieuwenburg, J. Gudat, S. Thon, H. Kim, M. P. van Exter, and D. Bouwmeester, *Phys. Rev. B* **84**, 075306 (2011).
 - [79] R. Albrecht, A. Bommer, C. Deutsch, J. Reichel, and C. Becher, *Phys. Rev. Lett.* **110**, 243602 (2013).
 - [80] Y. F. Xiao, C. L. Zou, P. Xue, L. X. Xiao, Y. Li, C. H. Dong, Z. F. Han, and Q. H. Gong, *Phys. Rev. A* **81**, 053807 (2010).
 - [81] L. M. Liang and C. Z. Li, *Phys. Rev. A* **72**, 024303 (2005).
 - [82] O. Zilberberg, B. Braunecker, and D. Loss, *Phys. Rev. A* **77**, 012327 (2008).